



# Machining deformation prediction of large fan blades based on loading uneven residual stress

Changfeng Yao<sup>1</sup> · Jiyin Zhang<sup>1</sup> · Minchao Cui<sup>1</sup> · Liang Tan<sup>1</sup> · Xuehong Shen<sup>1</sup>

Received: 10 January 2020 / Accepted: 7 April 2020 / Published online: 27 April 2020  
© Springer-Verlag London Ltd., part of Springer Nature 2020

## Abstract

Fan blade is an important component of turbofan engine. It is a kind of curved thin-walled structural parts, which tends to have a certain amount of deformation after machining process. In order to predict the deformation of fan blade after machining process, the commercial simulation software Abaqus® is used to analyze the deformation of fan blade with titanium alloy through considering the effect of residual stress. The residual stresses on the surface and subsurface of the blade after milling and shot peening processes were measured and analyzed by experimental testing. Based on the measured residual stress data, the three-dimensional model of fan blade is segmented by the operation of extracting geometric features. Then, the residual stress values are discretized according to separation layers, and the discrete results are applied to the thin-walled blade by dividing layers and dividing regions. Finally, a finite element analysis (FEA) model for the deformation prediction of blade through considering the effect of residual stress is established. The simulation deformation is compared with the measured deformation, and the feasibility of the FEA model is verified. The study provides an effective analysis method for the deformation prediction of fan blade after milling and shot peening processes.

**Keywords** Fan blade · Residual stress · Dividing layers · Dividing regions · Deformation prediction

## 1 Introduction

The turbofan engines have been developed to meet the requirements of modern aero engines, such as weight reduction, increasing thrust, reduction of fuel consumption, and noise control. As an important part of the turbofan engine, the fan blade is characterized by a long blade body (600 mm ~ 700 mm)

with a large twist angle. The complex structure of the fan blade significantly increases the difficulty and cost of blade machining. The performance of turbofan engines, such as safety, efficiency, reliability, and service life, is remarkably influenced by the precise shape and dimension of the fan blade.

With the development of science and technology, the application of finite element analysis (FEA) in the field of manufacturing is becoming more and more widespread [1–4]. Based on the analyses of the machining deformation mechanism and basic machining deformation characteristics of the thin-walled workpieces, Yan et al. [5] have presented an NC milling deformation–forecasting approach based on CAD/CAM/FEA integration to forecast the machining deformation of the aeronautical thin-walled workpieces. Based on the finite element software AdvantEdge®, WANG et al. [6, 7] have established an FEA model for the milling process of workpiece. Then, tool temperature, tool stress, and the elastic deformation of the free-form thin-walled blade were calculated, and the law of elastic deformation was predicted. Li et al. [8] have proposed a new iterative FEA model: the calculation of the interaction between deformation degree and cutting force. The mesh was very densely divided, and the cutting force was scattered on each node as the actual situation. Although there were still some errors, the simulated

✉ Changfeng Yao  
chfyao@nwpu.edu.cn

Jiyin Zhang  
zhangjiyin.chn@hotmail.com

Minchao Cui  
cuiminchao@nwpu.edu.cn

Liang Tan  
tanliang@nwpu.edu.cn

Xuehong Shen  
xuehua1323@163.com

<sup>1</sup> School of Mechanical Engineering, Northwestern Polytechnical University, Box 552, Xi'an 710072, Shaanxi, People's Republic of China

results are roughly consistent with the actual deformation. Liu et al. [9] have proposed a new method for predicting milling error based on FEA. The dynamic model of the tool was established, and the continuous machining process and milling error of arbitrary point were analyzed. The accuracy of the FEA method is verified by experiments. Based on FEA and force-model of Ti-6Al-4V alloy thin-wall components, Chen et al. [10] have predicted the machining deformation and compared with the measured data. Fei et al. [11] have studied the deformation of thin-walled structures during side milling. The cantilever plate was used as the object, and the classical equation was used to construct the motion equation of the component, then the state superposition method was used to solve the equation and obtain the deformation results. A three-dimensional FEA model has been established by Wang et al. [12] through considering the coupling effect of residual stress, milling force and clamping force on the machining deformation. The FEA of the cutting process from blank to workpiece was carried out, and the deformation of the sidewall during the machining process was obtained. Using finite element method, Cheng et al. [13] have analyzed the deformation law and cutting force variation of thin-walled parts. The correctness of the cutting force model is verified by the machining experiment of thin-walled parts. Ou et al. [14] have proposed a deformation prediction method based on back propagation neural network. The experimental results were obtained by orthogonal experimental design, and a neural network model for deformation prediction based on experimental results was established. The results showed that the deformation prediction model was reasonable and can be used for the prediction of milling deformation.

Scholars have done a lot of research on shot peening. Wang et al. [15] have studied the deformation of 7150 aluminum alloy specimens by changing the coverage of shot peening. The results showed that the curvature radius increased with the increase of the sheet thickness after shot peening. In addition, enhanced shot peening coverage can increase the deformation without changing the thickness and shot parameters. Achintha et al. [16] have presented a hybrid explicit finite element/eigenstrain model for predicting the residual stress generated by arrays of adjacent/overlapping laser shock peening shots. The prediction results for the strain distributions are in agreement with experimental measurements of plastic strain obtained by neutron diffraction. Gallitelli et al. [17] have studied the relation between the process parameters and the material state (residual stress and plastic variables) for complex geometry, and a finite element method was used to analyze the residual stress and deformation fields in the mechanical part. Salvati et al. [18] have proposed a particular way of prescribing the eigenstrain field due to surface treatment such as shot peening. The eigenstrain variation is described by a continuous function of the distance from the boundary of the object in a two-dimensional model of its cross-section, and the eigenstrain modeling approach generates an efficient parametric representation of the residual stress field.

The deformation problem of thin-walled workpieces during the manufacturing process is worth discussing. At present, most of the studies on the deformation of thin-walled structures are focused on the flat plates. In the previous studies of residual stress and deformation, the simulation was carried out based on uniform residual stresses, which is inconsistent with the actual residual stress distribution. In this paper, the uneven residual stresses are loaded to the different layers and regions, and then the research is carried out. The thin-walled blade with Ti-6Al-4V titanium alloy is taken as the research object. Based on the combination of FEA and experiment, the effects of residual stress on deformation of the thin-walled blade after milling and shot peening processes are studied. Firstly, the residual stress on the surface and subsurface of the blade after milling and shot peening are measured by an X-ray diffractometer, and the residual stress data were simply analyzed. Then the three-dimensional model of fan blade is divided by layers, and the measured residual stress is discretized corresponding to the division layers. Finally, the residual stress is applied to the three-dimensional model of fan blade by dividing layers and dividing regions, and the FEA is carried out to predict the deformation of the blade.

## 2 Finite element modeling and experimental measuring

### 2.1 Characteristics of the blade profile

The structure of the fan blades is complex. As shown in Fig. 1, the outer contour of the fan blade is composed of three-dimensional free surfaces. The curvature radius of the profile

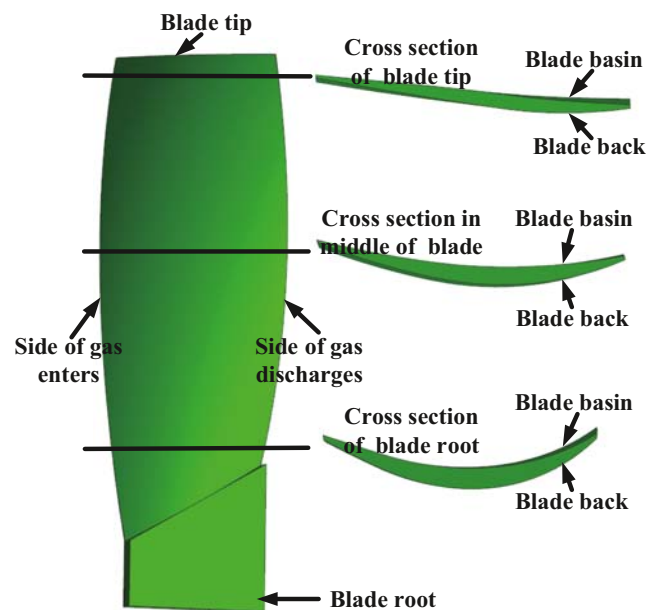


Fig. 1 The blade profile

near the root is small, but the curvature radius near the top of the blade is much larger than the root. The curvature radius is generally reduced from the top region to the root region. A large difference in curvature of the root of blade, the middle of blade, the top of blade, the side of gas enters, and the side of gas discharges. It also can be seen from different cross-sections that the thickness of each area of blade profile is inconsistent, which leads to a great difference in stiffness. In order to ensure the authenticity of residual stress distribution and improve the accuracy of the FEA model, the blade must be divided into several regions for analysis.

## 2.2 Finite element model of residual stress-induced deformations of blade

The size of blade model is big which is about 150 mm × 600 mm, and the blade profile is complicated. The curvature of blade differs greatly, and the thickness of each region of blade profile is inconsistent, which leads to a great difference in stiffness among the regions. If the same residual stress is loaded onto the surface of blade, the simulation accuracy is greatly reduced. In order to make the loading of residual stress closer to the real situation, and considering the time that is required by the FEA model, the blade surface is divided into nine regions as much as possible according to the principle of equal area, as shown in Fig. 2 a. The 18 measuring points of residual stress corresponds to the 18 divided regions of the blade. When the residual stresses are loaded, the residual stress values of each measuring point can be assigned to the corresponding region.

In the FEA process, the measured residual stress needs to be loaded into FEA model, and it is known that the residual stresses are distributed in the form of a curve along the depth direction. If these residual stresses are simply loaded during the FEA, it leads to the errors for the analysis of the residual stress-induced deformations. Therefore, the method of loading residual stresses by dividing layers is adopted in the present study, and the measured residual stresses are discrete according to the depth of each layer, then they are loaded layer by layer into FEA model. It makes the loaded residual stresses close to the actual residual stresses on the workpiece, thus ensuring the accuracy of the FEA.

The process of loading residual stresses layer by layer is shown in Fig. 2 b. Taking the milled blade as an example, the nine measurement points of the blade back or the blade basin were peeled five times in the depth direction, each at 10 μm, and each measurement point obtained six residual stress data (including surface residual stress), which are  $\sigma_0$ ,  $\sigma_1$ ,  $\sigma_2$ ,  $\sigma_3$ ,  $\sigma_4$ , and  $\sigma_5$ . In the FEA model, five sheets, namely  $l_1$ ,  $l_2$ ,  $l_3$ ,  $l_4$ , and  $l_5$ , are respectively tied to the blade back or blade basin, and the thickness of each sheet is 10 μm, which is the same as the thickness of each peeling layer. Then take the first area M-back-1 as an example,  $\sigma_{l1} = 0.5 \times (\sigma_0 + \sigma_1)$ ,  $\sigma_{l2} =$

$0.5 \times (\sigma_1 + \sigma_2)$ ,  $\sigma_{l3} = 0.5 \times (\sigma_2 + \sigma_3)$ ,  $\sigma_{l4} = 0.5 \times (\sigma_3 + \sigma_4)$ , and  $\sigma_{l5} = 0.5 \times (\sigma_4 + \sigma_5)$ , and  $\sigma_{l1}$ ,  $\sigma_{l2}$ ,  $\sigma_{l3}$ ,  $\sigma_{l4}$ , and  $\sigma_{l5}$  is the residual stress of each sheet. Therefore, the residual stress in the depth direction is discrete, that is, the residual stress loaded on the  $l_1$  layer is  $\sigma_{l1}$ , the residual stress loaded on the  $l_2$  layer is  $\sigma_{l2}$ , ..., and the remaining areas such as M-back-2, M-back-3, ..., M-basin-1, ..., and M-basin-9 are all the same. The distribution of measured residual stresses along the depth direction is discretized according to the thickness of each layer, and then the corresponding average stress of each layer is obtained. The residual stress values of each layer are respectively loaded onto the corresponding layers of the finite element model.

The residual stress belongs to the stress field, and the predefined field option should be set when loaded with residual stress. In the editing interface of the predefined field, each region of each layer is selected, and the corresponding residual stress is inputted. The residual stress values of a plurality of regions (90 regions of the milled blade, 128 regions of the blade after shot peening) were loaded one by one in this way, as shown in Fig. 2.

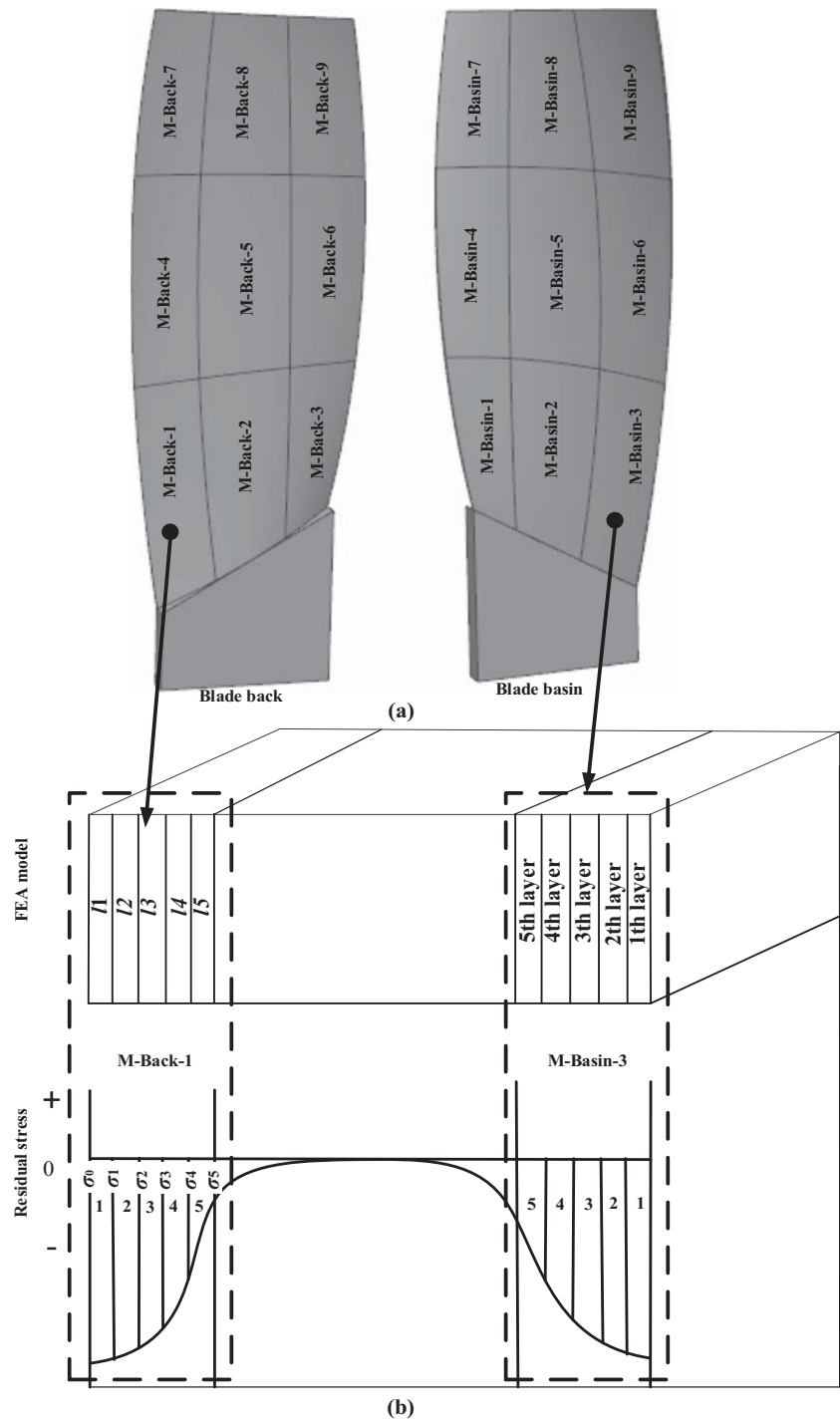
## 2.3 Machining of blades and measuring of residual stress

The material of fan blade is Ti-6Al-4V and after the blade was milled from blank, it was polished, heat-treated, and finally shot peening, and the blade will be polished again if the surface roughness is not satisfactory [19]. This paper mainly studies the residual stress-induced deformations after blade milling and shot peening. The milling process was completed on the DMU125P five-axis machining center of Gildemeister, and the shot peening was finished on the MP1500TX shot peening machine of Wheelabrator. The shot peening strength is 0.25 N, the pressure is 2 bar, the flow rate is 1.5 kg/min, and the moving speed is 600 mm/min, coverage  $\geq 100\%$ .

In this paper, the residual stress was measured using the PROTO-LXRD MG2000 residual stress measuring system, and the measuring interface was shown in Fig. 3. As shown in Fig. 3 a, the data of 18 points are fitted, and the fitting effect is well; therefore, the residual stress data is accurate. Figure 3 b shows that the diffraction peaks were detected on two probes, the diffraction peak fitting effect is well, and the reliability of the measured residual stress data is proved together with Fig. 3 a.

In order to obtain the distribution of residual stress along the depth, the residual stress data under the surface of blade should be measured. The blade was etched in a direction perpendicular to the surface using an electrolytic polisher and then the residual stress of each layer was measured. In the process of measuring the residual stress under the surface, etching the material layer by layer will release residual stress partly in depth of the workpiece, which will cause deformation at the same time, but the

**Fig. 2** Loading residual stress (take milled blade as an example): **a** the schematic diagram of dividing regions for blade and **b** the schematic diagram of dividing layers for blade



diameter of peel area is only 5 mm, and the blade is 150mm × 600mm, as shown in Fig. 4. The residual stress measurement system automatically calculates the “actual residual stress” as we enter the thickness and diameter of the etched region into the system, and the “actual residual stress” and deformation are affected little by etching.

Considering various factors, the parameters for measuring the residual stress of Ti-6Al-4V are as follows: voltage is

25 kV, current is 20 mA, x-ray transistor is Cu\_K-Alpha,  $\beta$  angle is  $\pm 25^\circ$ , diffraction crystal plane is {213}, Bragg angle  $2\theta$  is  $142^\circ$ , the number of exposures is 10, the exposure time is 2 s, and the diameter of the collimator is 3 mm.

In the measured data of residual stress, it can be found that there is an error in each measured data, but the error is only about  $\pm 20$  MPa, so it will be ignored in the analysis process and FEA model.

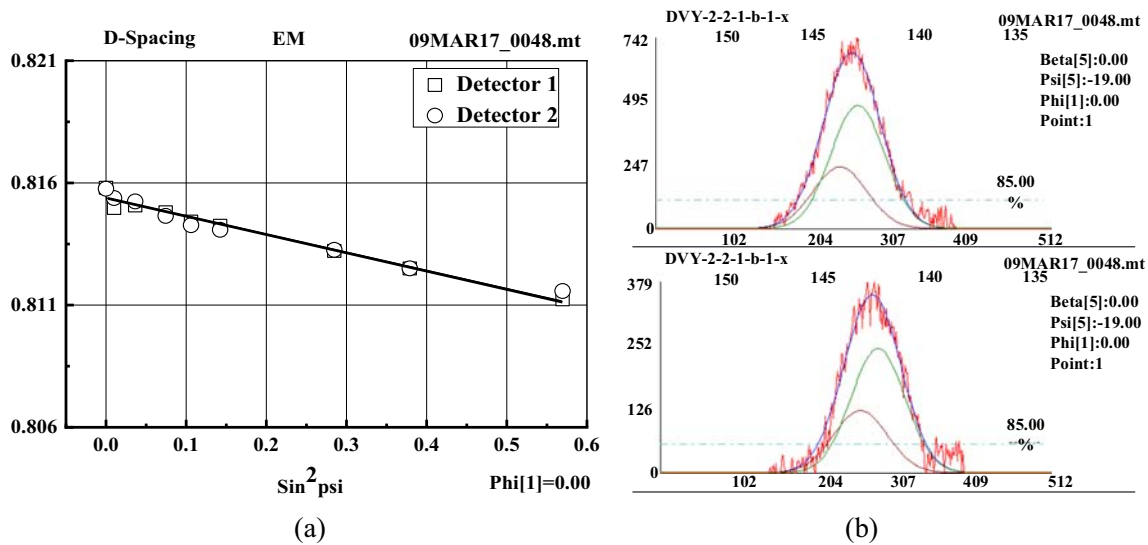


Fig. 3 Measuring interface of residual stress: **a** fitting of measurement points and **b** diffraction peaks

In order to make the measured residual stress reflect the residual stress distribution of blade as much as possible, the measurement points should be planned. The distribution of measurement points should be as uniform as possible and correspond to the division area of blade. For the convenience of analysis, the coordinate system of measurement points is consistent with the design model. The midpoint of the blade root is the origin point, from the side of gas enters to the side of gas discharges is the X-direction, from blade back to blade basin is the Y-direction, and from the root of blade to the tip of blade is the Z-direction.

### 2.4 Finite element analysis of residual stress-induced deformations

The geometry model of blade and sheets were imported into the Abaqus software, and the coordinate system in Abaqus software was consistent with the design coordinate system of the blade.

The material property parameters of Ti-6Al-4V were entered in the “property” module. The thickness of each sheet was set according to the depth of etch region, so the sheet’s thickness of the milled blade was 10  $\mu\text{m}$ , and the sheet’s thickness of the

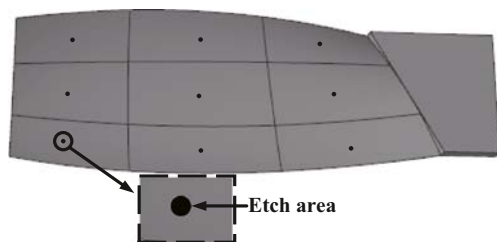


Fig. 4 Etch area of blade: take one of the nine etch areas on the blade back as an example

blade after shot peening was 30  $\mu\text{m}$ . In order to match the direction of the loaded residual stress with the direction of the measured residual stress, it is necessary to set the material direction for each sheet. The Z-direction and the X-direction of residual stress as shown in Fig. 5, and the direction perpendicular to the surface is the Y-direction of residual stress.

The deformation analysis of the blade is based on the root of the blade, so the root of blade model should be constrained when establishing boundary conditions. The boundary constraint of blade root is “encased”, and the six degrees of freedom of blade root are completely constrained.

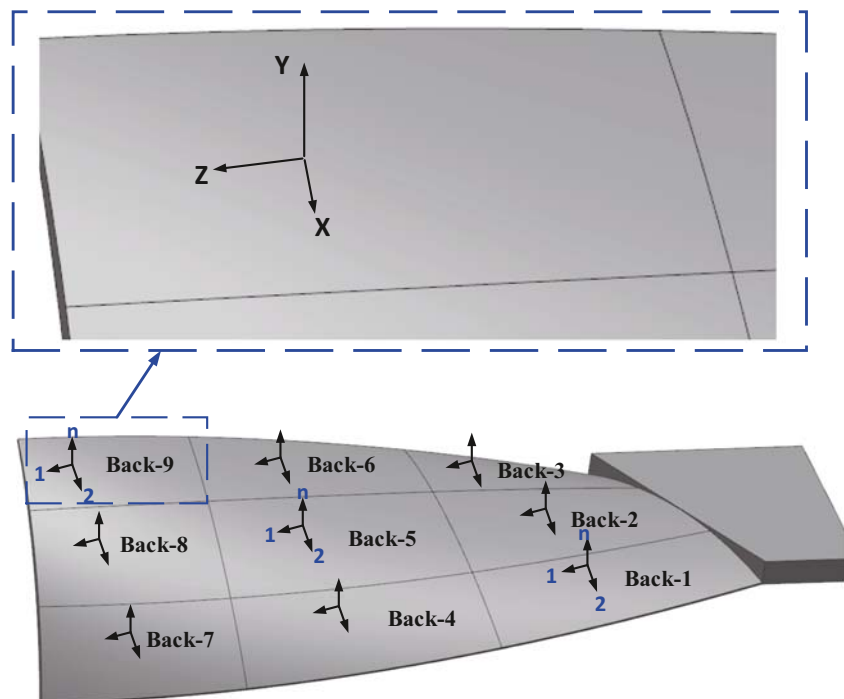
In this paper, the residual stress-induced deformations of the blade after milling and shot peening are studied. The measured residual stresses are the residual stress after blade was deformed. The residual stress that was loaded into the FEA model should be converted to the stress before the blade deformed. In order to explore their differences, the same compressive residual stresses in the X-direction and Z-direction were loaded onto the back and basin of blade. A plurality of points were randomly selected on the back and basin of the deformed blade to measure residual stress and obtain the residual stress values after deformed blade.

The different level residual stress values of the random points after blade deformed were statistically analyzed, and the comparison with the residual stress before the blade deformed is shown in Table 1.

It can be seen from Table 1 that the residual stress value changes before and after the blade deformed, and the compressive residual stresses are reduced by 2 ~ 3%. Therefore, the measured residual stresses need to be processed, and the measured residual stresses after blade deformed should be converted to the residual stresses before blade deformed.

The meshing is closely related to the analysis time and the accuracy of the FEA result. Excessive mesh size has low

**Fig. 5** Material direction: take one of the nine areas on the blade back as an example



analytical accuracy, and too small mesh size can prolong analysis time. After many experiments and explorations, a meshing method considering both analysis accuracy and time cost is adopted. The element size of the blade is 8 mm, the element type is C3D10, and the total number of elements is 20,136. The element size of the sheet is 8 mm, the element type is S4R, and the number of elements is 1765.

### 3 Results and discussion

#### 3.1 Residual stress of blade after milling and shot peening

The three-dimensional distribution of the residual stress on the blade back after milling is shown in Fig. 6, and the distribution of residual stress on the blade basin is consistent with blade back. Figure 6 a shows the distribution of residual stress on the surface. The X-axis and the Z-axis are the coordinate axes of the two-dimensional plane of the surface of the workpiece, and the residual stress values in various regions of the surface are presented by different colors. As can be seen from the figure, the residual stress at each point of the blade is greatly different.

Figure 6 b shows the distribution of residual stress along the depth direction at three certain points of the surface of the

workpiece. The point of A, B, and C respectively show the distribution of the low, medium, and high level of compressive residual stress along the depth direction. The abscissa represents the depth perpendicular to the surface direction, and the ordinate represents the compressive residual stress. The compressive residual stress on the surface is about  $-240$  MPa  $\sim$   $-400$  MPa, and then the compressive residual stress gradually decreases with the increase of depth, and finally decreases to about  $0$  MPa at a depth of  $40$   $\mu\text{m}$   $\sim$   $60$   $\mu\text{m}$ . The residual stress value of blade body is  $0$  MPa, which indicates that the depth of the residual stress field after the blade milling is about  $50$   $\mu\text{m}$ .

In previous research [20], it also can be seen that the distribution of the residual stress after milling along the direction perpendicular to the surface of the workpiece is non-uniform. For a real-milled workpiece, the machining process cannot be completed in an instant, but in a sequential one-to-one cutting process. As the material is continuously removed during the cutting process, the overall structure, the stiffness, and natural frequency are also changed. Meanwhile, the tool is also worn, and the temperature of the cutting area is also changed. All those changes generate different residual stresses in each region of the surface of the workpiece after machining.

The three-dimensional distribution of the residual stress on the blade basin after shot peening is shown in Fig. 7, and the distribution of residual stress on the blade back is consistent

**Table 1** Comparison of residual stress

Level	1	2	3	4	5	6
Residual stress before deformation (MPa)	-200	-300	-400	-500	-600	-700
Residual stress after deformation (MPa)	-196	-292	-390	-487	-585	-682

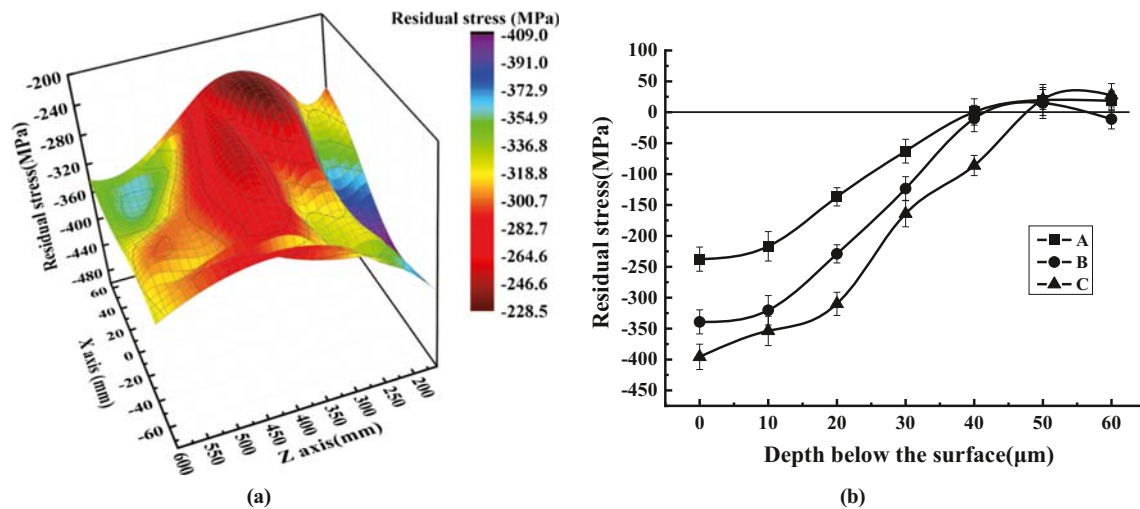


**Fig. 6** The distribution of residual stress after milling: **a** the distribution of residual stress on the surface and **b** the distribution of residual stress along the depth direction

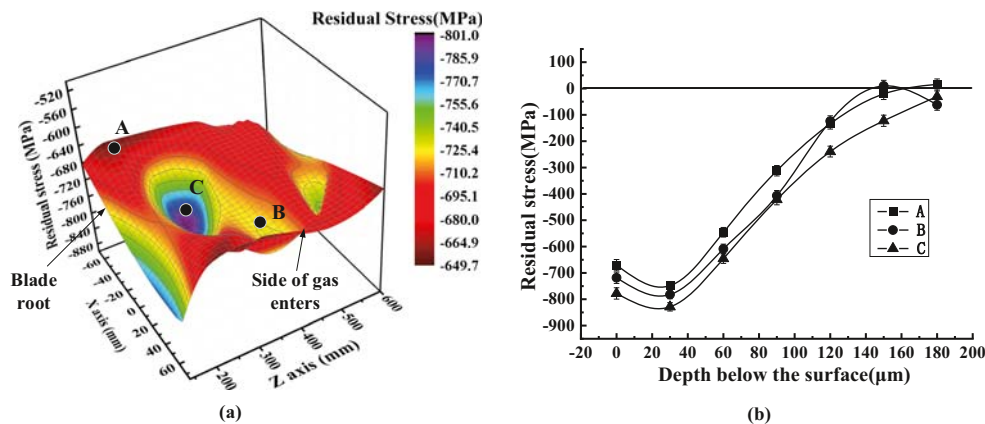
with blade basin. Figure 7 a shows the distribution of residual stress on the surface. It can be seen from the figure that the distribution trend of residual stress along the depth direction is generally uniform as the blade after milling.

Figure 7 b shows the distribution of residual stress at a certain point on the surface of the workpiece along the depth direction. The point of A, B, and C also respectively show the distribution of the low, medium, and high level of compressive residual stress along the depth direction. The compressive residual stress on the surface is about  $-660$  MPa to  $-770$  MPa. The maximum compressive residual stress value is reached at the depth of  $30\ \mu\text{m}$ , and then the compressive residual stress gradually decreases with the increase of the depth, and finally decreases to about  $0$  MPa at the depth of  $150\ \mu\text{m}$  and  $180\ \mu\text{m}$ .

In the previous research [21, 22], the residual stress after shot peening is distributed in a curved form along the direction perpendicular to the surface of the workpiece. For the real shot peening workpiece, the machining process cannot be

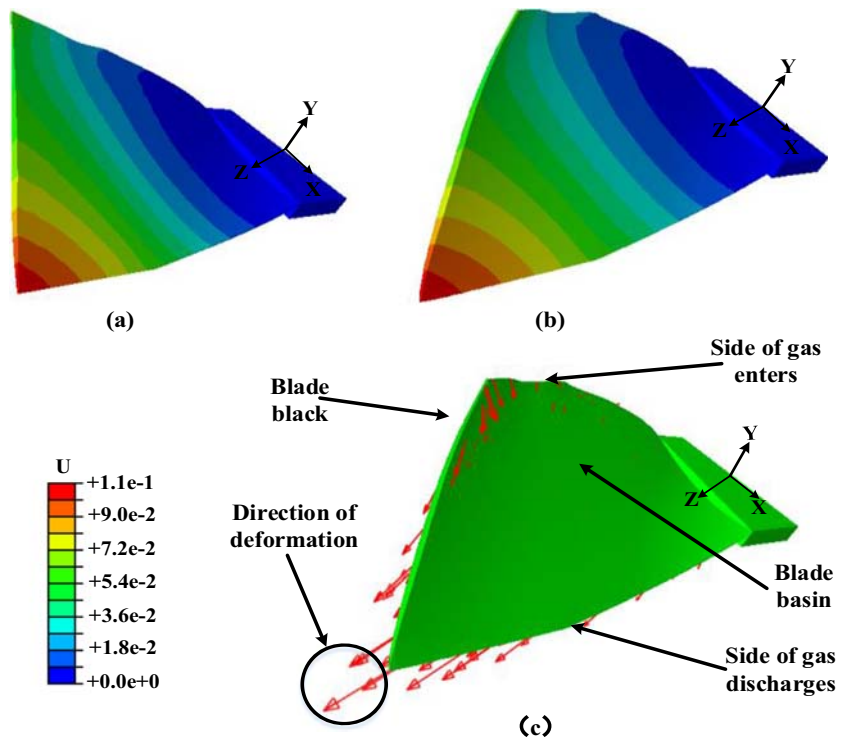
completed in an instant but is processed in a sequence along the planned path in a certain period of time. During the whole shot peening process, as the shot peening continues, the shot peening position is constantly changing, the rigidity of the thin-walled workpiece is also changing, and the subsequent shot peening process has the effect of vibratory stress relief on the shot-peened portion. This produces different residual stresses in different regions of the workpiece after manufacturing.

It can be seen from Figs. 6 and 7 that the residual stress at each point of blade back and blade basin are inconsistent in the depth direction after milling and shot peening processes, and they are also different at the same depth. Due to the uneven distribution of stress in the depth direction and the uneven distribution of the surface, the entire workpiece will reach equilibrium by deformation according to the principle of “force balance, torque balance.” This is the theoretical basis of the residual stress-induced deformations of the workpiece. For a workpiece with a larger size and a more complex structure, the deformation is more complicated. In order to reflect



**Fig. 7** The distribution of residual stress after shot peening: **a** the distribution of residual stress on the surface and **b** the distribution of residual stress along the depth direction

**Fig. 8** Simulated deformation of milled blade: **a** original blade, **b** deformed blade, and **c** trend of deformation



the distribution of the residual stress of the blade more realistically, the residual stress data should be applied to the FEA model by dividing layers and regions.

**3.2 Finite element analysis results**

The simulated deformation of the blade after milling are shown in Figs. 8, 9 and 10. It can be seen from Fig. 8 that the blade is deflected from blade basin toward the blade back with a certain degree of torsion. From Figs. 9 and 10, it can be

found that the deformation of section 2 was larger than that of section 1, and the largest deformation area of the blade was mainly concentrated on the tip of the blade. The blade was twisted in the positive direction of the Z-axis, and the deformation at the side where gas enters was smaller than the side where gas discharges. The maximum deformation amount of the X-direction is 0.10 mm, and the maximum deformation amount of the Y-direction is 0.08 mm.

The simulated deformation of the blade after shot peening are shown in Figs. 11, 12 and 13. It can be seen from Fig. 11

**Fig. 9** Deformation of milled blade of the X-direction: **a** original blade, **b** trend of deformation, and **c** section of the deformation model

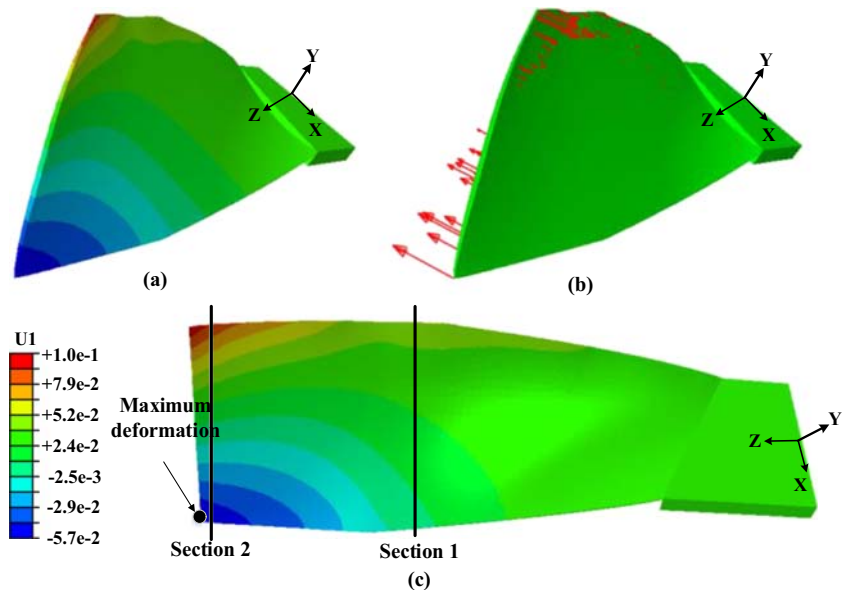
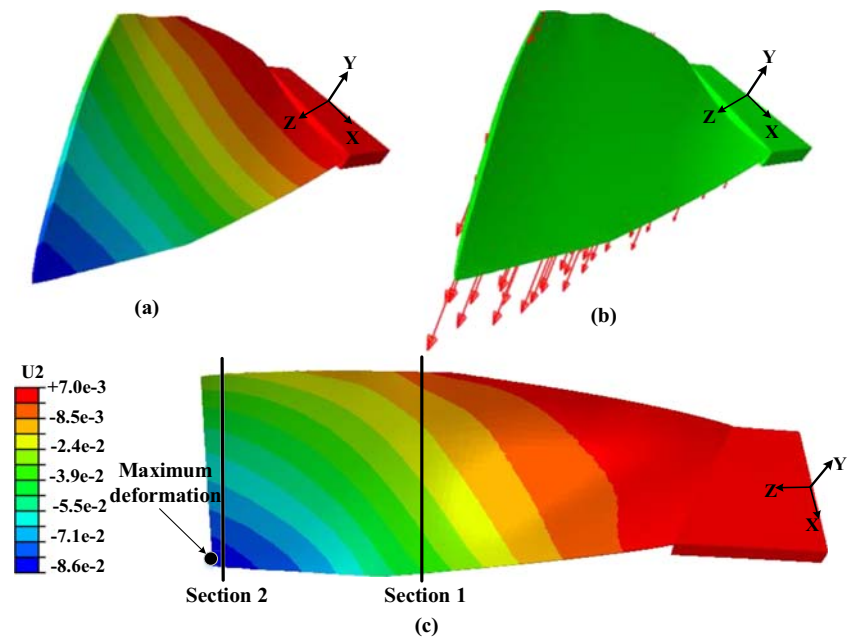




**Fig. 10** Deformation of milled blade of the Y-direction: **a** original blade, **b** trend of deformation, and **c** section of the deformation model



that the blade was deflected from the blade basin toward the blade back with a certain degree of torsion. However, at the top of the blade near the gas entry side, the blade back was deflected to the blade basin. From Figs. 12 and 13, it can be found that the deformation of section 2 was larger than that of section 1, and the largest deformation area of blade was mainly concentrated on the tip of the blade. The maximum deformation amount of the X-direction is 0.20 mm, and the maximum deformation amount of the Y-direction is 0.23 mm.

The deformation of section 1 and section 2 of the blade after milling and shot peening was measured on a three-coordinate measuring machine. The measured deformation and simulated deformation are shown in Fig. 14.

After analyzing the simulated results and measured results, it is found that the deformation of section 2 is larger than section 1, and the simulated value is smaller than the measured value, but the amounts of deformation are in the same order of magnitude. The material property parameters of Ti-6Al-4V in the FEA were searched from one study [23], so there may be some deviations in the real situation and FEA model, and it leads to some differences in the simulated results and measured results. The blade model is so big, and the element size is 8 mm, it also will cause the problem.

Although there are several differences in the simulated deformation and measured deformation, the difference is less than 25%. Comparing the simulated and measured

**Fig. 11** Simulated deformation of the blade after shot peening: **a** original blade, **b** deformed blade, and **c** trend of deformation

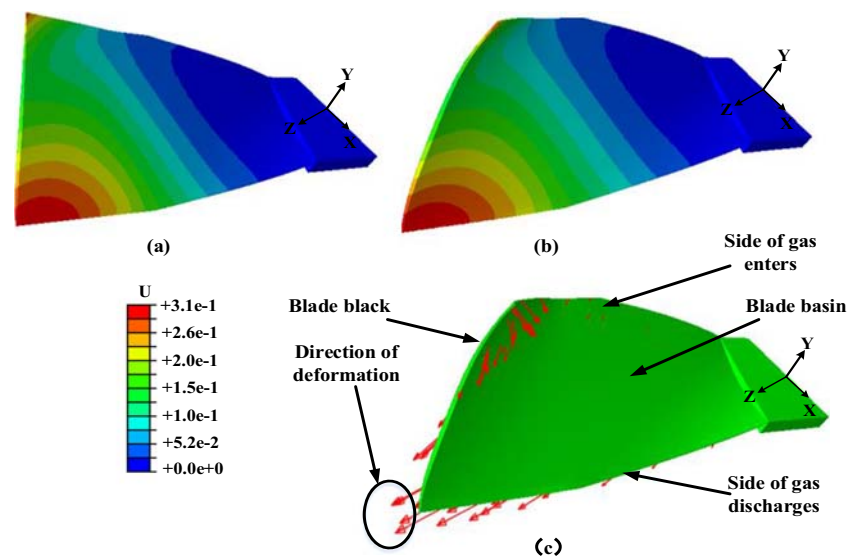
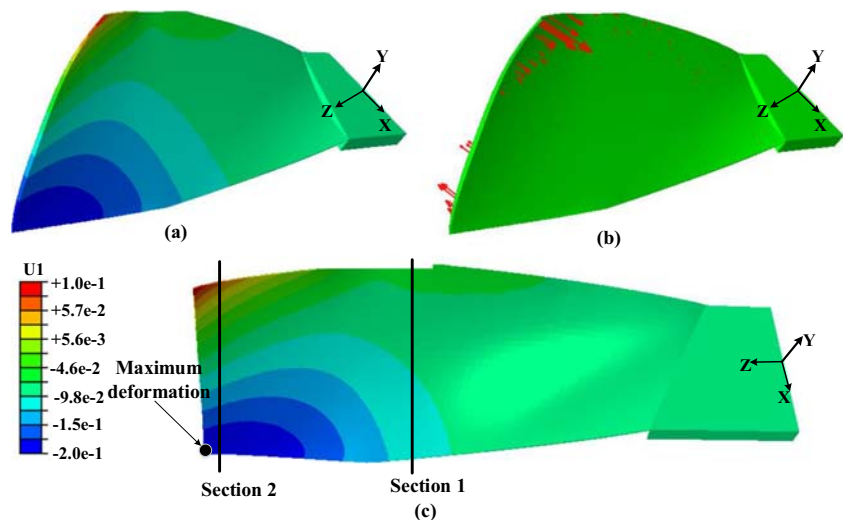


**Fig. 12** Deformation of blade after shot peening of the X-direction: **a** original blade, **b** trend of deformation, and **c** section of the deformation model



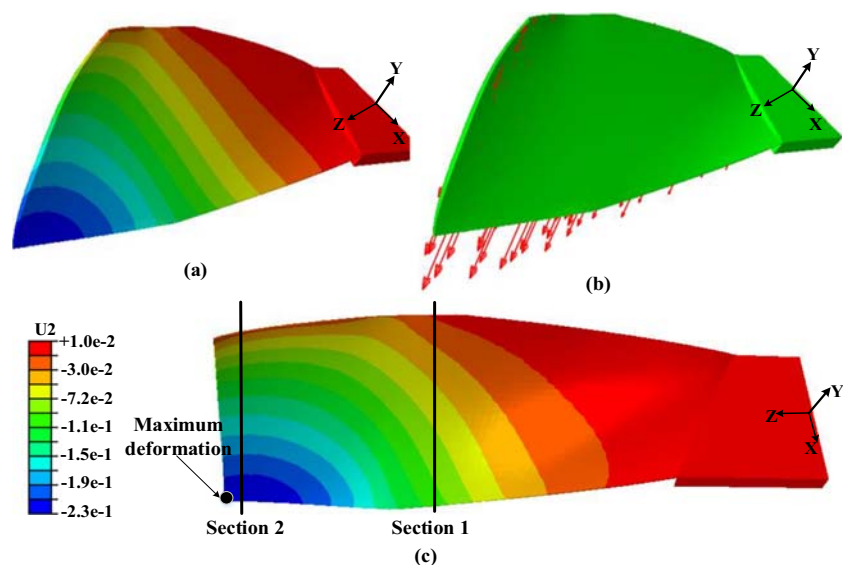
deformation trends of the blade, it is found that the simulated and measured distortion angles are all positive values, and the difference is small, which means that they are all twisted in the positive direction of the Z-axis. All these results show that the simulation results are consistent with experimental results though there remains a gap between simulation results and experimental testing results. This verifies the feasibility of the FEA model for the residual stress-induced deformations of the blade again. As the manufacturing cost of large fan blades is high and it takes a long time to manufacture, it is impractical to perform a large number of large fan blades milling and shot peening experiments to study the deformation problem. The FEA can be used as a research tool that requires little time and cost. Therefore, a series of simulation studies on residual stress and deformation of the blade can be carried out by the FEA, which provides a technical means for the simulation study of blade deformation caused by residual stress. We can study the effect of different residual stresses

between blade back and blade basin on deformation in the future.

## 4 Conclusion

- 1) The residual stresses on the surface and subsurface of the blade after milling and shot peening were measured and analyzed. Based on the measured residual stress data on the blade, the distribution of residual stress was analyzed. The maximum compressive residual stress of the milled blade is located at the surface, which is about  $-240$  MPa  $\sim -400$  MPa, and the compressive residual stress gradually decreases with the increase of depth until the depth of  $60\ \mu\text{m}$  drops to  $0$  MPa. The compressive residual stress on the blade after shot peening is about  $-660$  MPa  $\sim -770$  MPa, and the maximum compressive residual stress is about  $-750$  MPa  $\sim -840$  MPa at the depth of  $30\ \mu\text{m}$ .

**Fig. 13** Deformation of blade after shot peening of the Y-direction: **a** original blade, **b** trend of deformation, and **c** section of the deformation mod



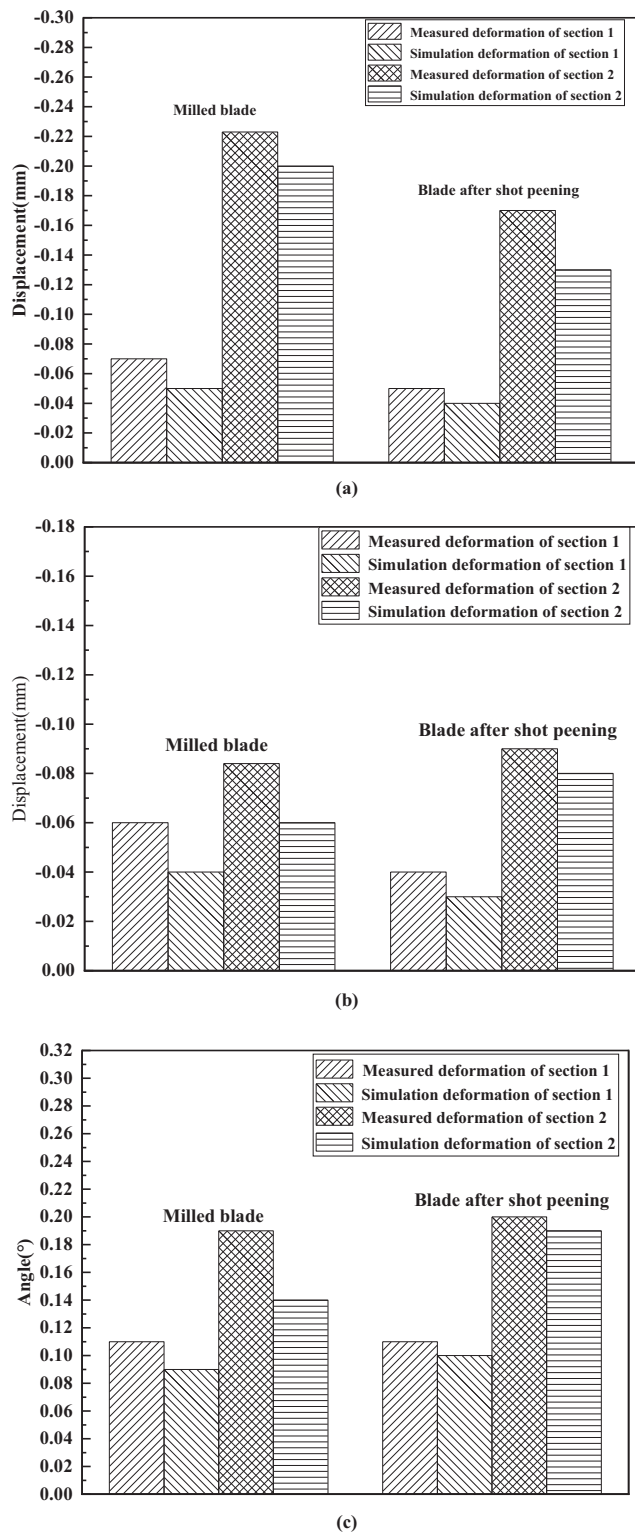


**Fig. 14** Deformation of the blade: **a** deformation of X-direction, **b** deformation of Y-direction, and **c** distortion

The compressive residual stress decreases with the increase of depth, and the compressive residual stress drops to 0 MPa when the depth is 160  $\mu\text{m}$ .

2) The FEA model for loading residual stress on the blade to simulate deformation was established. Comparing the simulation deformation results with the measured deformation results, it is found that the simulation deformation values have a certain deviation from the measurement results, but the deformation amount of simulation and measurement are in the same order of magnitude. The simulated deformation shows the consistent trend with the actual deformation, and both of them are twisted in the positive direction of the Z-axis. The feasibility of the FEA model, which is based on the uneven residual stress method, is verified. The method in this study not only provides a reference for the process control of the thin-walled structure manufacturing but also supplies an idea of the coordinated control of residual stress and deformation.

**Funding information** This work was funded by the National Natural Science Foundation of China (Grant Nos. 51875472, 51905440, and 91860206), the National Science and Technology Major Project (Grant No. 2017-VII-0001-0094) and the National Key Research and Development Plan in Shaanxi Province of China (Grant No. 2019ZDLGY02-03).

## References

- Pu X, Zhang C, Li S, Deng D (2017) Simulating welding residual stress and deformation in a multi-pass butt-welded joint considering balance between computing time and prediction accuracy. *Int J Adv Manuf Technol* 93(5–8):2215–2226
- Cui M-C, Zhao S-D, Zhang D-W, Chen C, Li Y-Y (2017) Finite element analysis on axial-pushed incremental warm rolling process of spline shaft with 42CrMo steel and relevant improvement. *Int J Adv Manuf Technol* 90(9–12):2477–2490
- Cui M-C, Zhao S-D, Zhang D-W, Chen C, Fan S-Q, Li Y-Y (2017) Deformation mechanism and performance improvement of spline shaft with 42CrMo steel by axial-infeed incremental rolling process. *Int J Adv Manuf Technol* 88(9–12):2621–2630
- Lu LX, Sun J, Li YL, Li JF (2017) A theoretical model for load prediction in rolling correction process of thin-walled aeronautic parts. *Int J Adv Manuf Technol* 92(9–12):4121–4131
- Cao Y, Bai Y, He Y, Tian J, Li Y (2014) NC milling deformation forecasting of aluminum alloy thin-walled workpiece based on orthogonal cutting experiments and CAD/CAM/FEA integration paper title. *IJCA* 7(9):67–80
- Wang L-y, H-h H, West RW, H-j L, J-t D (2018) A model of deformation of thin-wall surface parts during milling machining process. *J Cent South Univ* 25(5):1107–1115
- Wang L, Si H (2018) Machining deformation prediction of thin-walled workpieces in five-axis flank milling. *Int J Adv Manuf Technol* 97(9–12):4179–4193
- P-f L, Liu Y, Y-d G, L-l L, Liu K, Sun Y (2018) New deformation prediction of micro thin-walled structures by iterative FEM. *Int J Adv Manuf Technol* 95(5–8):2027–2040
- Si-meng L, Xiao-dong S, Xiao-bo G, Dou W (2017) Simulation of the deformation caused by the machining cutting force on thin-walled deep cavity parts. *Int J Adv Manuf Technol* 92(9–12):3503–3517

10. Chen TT, Rong B, Yang YF, Zhao W, Li L, He N (2014) FEM-based prediction and control of milling deformation for a thin-wall web of Ti-6Al-4V alloy. *MSF* 800-801:368–373
11. Fei J, Lin B, Yan S, Ding M, Zhang X, Zhang J, Lan J (2018) Theoretical prediction and experimental validation of dynamic deformation during machining of thin-walled structure. In: proceedings of the ASME International Mechanical Engineering Congress and Exposition – 2017: presented at ASME 2017 International Mechanical Engineering Congress and Exposition, November 3–9, 2017, Tampa, Florida, USA. The American Society of Mechanical Engineers, New York, NY, V002T02A004
12. Huang X, Sun J, Li J (2015) Finite element simulation and experimental investigation on the residual stress-related monolithic component deformation. *Int J Adv Manuf Technol* 77(5–8):1035–1041
13. Cheng Y, Zuo D, Wu M, Feng X, Zhang Y (2015) Study on simulation of machining deformation and experiments for thin-walled parts of titanium alloy. *IJCA* 8(1):401–410
14. Ouyang HB (2014) Deformation prediction based on BP artificial neural network of milling thin-walled aluminum alloy parts. *AMM* 687-691:492–495
15. Wang MT, Zeng YS, Bai XP, Huang X (2014) Deformation rule of 7150 aluminum alloy thick plate by pre-stress shot peen forming. *AMR* 1052:477–481
16. Achintha M, d. Nowell, Shapiro K, Withers PJ (2013) Eigenstrain modelling of residual stress generated by arrays of laser shock peening shots and determination of the complete stress field using limited strain measurements. *Surf Coat Technol* 216: 68–77
17. Gallitelli D, Boyer V, Gelineau M, Colaitis Y, Rouhaud E, Retraint D, Kubler R, Desvignes M, Barrallier L (2016) Simulation of shot peening: from process parameters to residual stress fields in a structure. *Comptes Rendus Mécanique* 344(4–5):355–374
18. Salvati E, Lunt AJG, Ying S, Sui T, Zhang HJ, Heason C, Baxter G, Korsunsky AM (2017) Eigenstrain reconstruction of residual strains in an additively manufactured and shot peened nickel superalloy compressor blade. *Comput Methods Appl Mech Eng* 320: 335–351
19. Huai W, Shi Y, Tang H, Lin X (2019) An adaptive flexible polishing path programming method of the blisk blade using elastic grinding tools. *J Mech Sci Technol* 33(7):3487–3495
20. Yao C, Tan L, Yang P, Zhang D (2018) Effects of tool orientation and surface curvature on surface integrity in ball end milling of TC17. *Int J Adv Manuf Technol* 94(5–8):1699–1710
21. Wu D, Yao C, Zhang D (2018) Surface characterization and fatigue evaluation in GH4169 superalloy: comparing results after finish turning; shot peening and surface polishing treatments. *Int J Fatigue* 113:222–235
22. Yao C, Wu D, Ma L, Tan L, Zhou Z, Zhang J (2016) Surface integrity evolution and fatigue evaluation after milling mode, shot-peening and polishing mode for TB6 titanium alloy. *Appl Surf Sci* 387:1257–1264
23. Liu C, Goel S, Llavori I, Stolf P, Giusca CL, Zabala A, Kohlscheen J, Paiva JM, Endrino JL, Veldhuis SC, Rabinovich F, German S (2019) Benchmarking of several material constitutive models for tribology, wear, and other mechanical deformation simulations of Ti6Al4V. *J Mech Behav Biomed Mater* 97:126–137

**Publisher's note** Springer Nature remains neutral with regard to jurisdictional claims in published maps and institutional affiliations.